

# Diagonal Padé approximant of the one-body Green's function: A study on Hubbard rings

Walter Tarantino\*

*Materials Theory, ETH Zürich, Wolfgang-Pauli-Strasse 27, CH-8093 Zürich, Switzerland  
and Laboratoire des Solides Irradiés, Ecole Polytechnique, CNRS, CEA, Université Paris-Saclay, F-91128 Palaiseau, France*

Stefano Di Sabatino

*Laboratoire des Solides Irradiés, Ecole Polytechnique, CNRS, CEA, Université Paris-Saclay, F-91128 Palaiseau, France*



(Received 9 November 2018; published 25 February 2019)

Padé approximants to the many-body Green's function can be built by rearranging terms of its perturbative expansion. The hypothesis that the best use of a finite number of terms of such an expansion is given by the subclass of *diagonal* Padé approximants is here tested, and largely confirmed, on a solvable model system, namely the Hubbard ring for a variety of site numbers, fillings, and interaction strengths.

DOI: [10.1103/PhysRevB.99.075149](https://doi.org/10.1103/PhysRevB.99.075149)

## I. INTRODUCTION

In the context of quantum field theory, perturbation theory allows us to derive a formal series for the interacting one-body Green's function in terms of the corresponding noninteracting one. In an oversimplified notation this reads

$$G = G_0 + G_0 v G_0 G_0 + G_0 v G_0 G_0 v G_0 G_0 + \dots, \quad (1)$$

where  $v$  denotes the interaction between the particles. Convergence properties of this series depend on the specific Hamiltonian one starts from; for most interesting cases the series is suspected to be, however, either divergent or merely slowly convergent. A way to overcome this limit is to sum up an infinite subset of terms, which is commonly achieved by recasting the calculation of  $G$  in the form of a Dyson equation:

$$G = G_0 + G_0 \Sigma G, \quad (2)$$

where  $\Sigma$ , the so-called self-energy of the system, has itself a (simpler) perturbative expansion in terms of  $G_0$  and  $v$ , which leads to the following expansion of the Green's function:

$$G = (G_0^{-1} - v G_0 - v G_0 v G_0 G_0 - \dots)^{-1}. \quad (3)$$

A finite number of terms of the expansion of  $\Sigma$  results in an infinity of terms for the corresponding approximate  $G$  and it usually greatly improves over the approximation provided by (1). Such an expansion is at the heart of state-of-the-art methods used nowadays for the estimate of  $G$  for real systems [1].

One way to explain this success is to interpret the approach in terms of Padé approximants [2]. Given a certain function  $f(z)$ , if we only know the first  $n + 1$  coefficients of its Taylor expansion  $f(z) = c_0 + c_1 z + c_2 z^2 + \dots + c_n z^n + \dots$ , we can approximate the function with a power series that gives rise to the same expansion, which is trivially the  $n$ th order truncation of the Taylor series itself,  $f(z) \approx c_0 + c_1 z + c_2 z^2 + \dots + c_n z^n$ . This is what standard perturbation theory does. Alternately,

we can use the rational function

$$\frac{a_0 + a_1 z + a_2 z^2 + \dots + a_p z^p}{1 + b_1 z + b_2 z^2 + \dots + b_q z^q} \quad (4)$$

whose coefficients are determined by the same condition, namely that (4) gives rise to the same Taylor expansion of  $f(z)$  up to the  $n$ th order. For given  $n$  this criterion identifies not just one but a set of rational functions obtained for different values of  $p$  and  $q$  with the constrain  $p + q = n$ ; these functions are called 'Padé approximants' of order  $p$  and  $q$  and denoted by  $[p/q]_f(z)$ , or, in short,  $[p/q]$ . The special case  $p = q$  is called *diagonal* Padé approximant. The approximant  $[n/0]$  is the truncated Taylor series itself, hence the series of Padé approximants can be considered as a way to generalize the Taylor series. For many functions, Padé approximants are found to represent better approximations than truncations of the Taylor series [3]. Perhaps not surprisingly, this is particularly true when the series diverges: A divergence in the Taylor expansion of a function reflects the presence of singularities over the complex plane  $z \in \mathbf{Z}$  which a power series representation is incapable to describe; a rational function, on the other hand, has singularities of its own which can be 'tuned' to fit those of the function to approximate. If the Green's function was simply a function of  $v$ , the series generated by perturbation theory (1) would amount to its Taylor expansion, or, in terms of Padé approximants,  $[n/0]$ , while solving the Dyson equation with the  $n$ th truncation of the perturbative expansion of  $\Sigma$  would represent a Padé approximant  $[0/n]$  (the fact that the Green's function in facts depends on spin/space/time variables makes the definition of Padé approximants less obvious than its Taylor expansion, as we shall later see). From this perspective, it is then natural to expect that, if the perturbative series for the actual Green's function seems to diverge, solving the Dyson equation with a perturbative self-energy may then give rise to a sequence of approximations with better convergence properties, as it turns out to be in many cases of interest.

In fact, one can go one step farther. As mentioned, for a given order of truncation of the Taylor expansion there is a

\*walter.tarantino@mat.ethz.ch



$$= (\mathbb{I} - \lambda(\mathbf{G}_1\mathbf{G}_0^{-1} - \lambda(\mathbf{G}_1\mathbf{G}_0^{-1}\mathbf{G}_1\mathbf{G}_0^{-1} - \mathbf{G}_2\mathbf{G}_0^{-1}) + \dots))^{-1}\mathbf{G}_0 \quad (11)$$

$$= (\mathbb{I} - \lambda(\mathbf{G}_0\mathbf{G}_1^{-1} + \lambda(\mathbb{I} - \mathbf{G}_0\mathbf{G}_1^{-1}\mathbf{G}_2\mathbf{G}_1^{-1}) + \dots)^{-1})^{-1}\mathbf{G}_0 \quad (12)$$

where we inverted series between parenthesis twice; a truncation of the series in the last line yields

$$\mathbf{G} \approx (\mathbb{I} - \lambda(\mathbf{G}_0\mathbf{G}_1^{-1} + \lambda(\mathbb{I} - \mathbf{G}_0\mathbf{G}_1^{-1}\mathbf{G}_2\mathbf{G}_1^{-1}))^{-1})^{-1}\mathbf{G}_0 \quad (13)$$

which is a generalization of (5) for the matrix  $\mathbf{G}$ . If  $\mathbf{G}$  is written in terms of a Dyson equation  $\mathbf{G} = \mathbf{G}_0 + \mathbf{G}_0\mathbf{\Sigma}\mathbf{G}$ , with  $\mathbf{\Sigma} = \lambda\mathbf{\Sigma}_1 + \lambda^2\mathbf{\Sigma}_2 + \dots$ , the above procedure leads to

$$\mathbf{\Sigma} \approx \lambda(\mathbf{\Sigma}_1^{-1} - \lambda\mathbf{\Sigma}_1^{-1}\mathbf{\Sigma}_2\mathbf{\Sigma}_1^{-1})^{-1}. \quad (14)$$

Actual Green's functions depend on two spin-space-time coordinates rather than just two discrete, finite indices, but the generalization of the above is straightforward:

$$G(1, 2) \approx \left( G_0^{-1}(1, 2) - \left( \Sigma_1^{-1}(1, 2) - \int d3d4 \Sigma_1^{-1}(1, 3)\Sigma_2(3, 4)\Sigma_1^{-1}(4, 2) \right)^{-1} \right)^{-1} := P_{[1/1]}[G_0(1, 2)] \quad (15)$$

or, equivalently,

$$\Sigma(1, 2) \approx \left( \Sigma_1^{-1}(1, 2) - \int d3d4 \Sigma_1^{-1}(1, 3)\Sigma_2(3, 4)\Sigma_1^{-1}(4, 2) \right)^{-1} \quad (16)$$

where  $G$  is the Green's function,  $G_0$  its noninteracting counterpart,  $\Sigma$  the self-energy,  $\Sigma_1, \Sigma_2$ , being the first terms of its perturbative expansion of order 1 and 2, and the notation 1,2,... shorthands their spin/space-time dependence  $(\sigma_1, \mathbf{r}_1, t_1), (\sigma_2, \mathbf{r}_2, t_2), \dots$ . A specific symbol for the approximant [1/1] as functional of the noninteracting Green's function,  $P_{[1/1]}[G_0]$ , has been introduced. More precisely, this is equivalent to  $[1/1]_G[\lambda]$  with  $\lambda$ , the parameter that in G-PT is formally introduced to derive the equivalent of (8), set to 1. This notation emphasizes the fact that we start from a given noninteracting Green's function  $G_0$  (which encodes the information of the parameter  $\lambda$  via  $\lim_{\lambda \rightarrow 0} G = G_0$ ). Since in the calculation of electronic structures it is customary to build perturbative approximations upon mean-field ones, like Hartree, Hartree-Fock or DFT, this notation allows us to clearly specify which noninteracting Green's function we start from (for instance  $P_{[1/1]}[G_0^{(0)}]$ ,  $P_{[1/1]}[G_H]$ , or  $P_{[1/1]}[G_{\text{LDA}}]$  for a completely free, a Hartree, or a DFT Green's function in the local density approximation, respectively). The choice of  $G_0$  also determines the exact forms of  $\Sigma_1$  and  $\Sigma_2$ . If  $G_0$  is the Green's function corresponding to the Hamiltonian  $H_0 = T + V_{\text{ext}} + V_{m.f.}$ , where  $T$  is the kinetic term, and  $V_{\text{ext}}$  and  $V_{m.f.}$  are the terms that couple the electronic field to the external and the mean-field potential,  $v_{\text{ext}}(\vec{r})$  and  $v_{m.f.}(\vec{r})$ , respectively,  $\Sigma_1$  and  $\Sigma_2$  are given, diagrammatically, by

$$\Sigma_1 = \text{[diagram 1]} + \text{[diagram 2]} + \dots \quad \text{and} \quad \Sigma_2 = \text{[diagram 3]} + \text{[diagram 4]} + \text{[diagram 5]} + \text{[diagram 6]} + \text{[diagram 7]} + \text{[diagram 8]} + \text{[diagram 9]} + \text{[diagram 10]}, \quad (17)$$

where straight lines represent  $G_0$ , wiggly lines the two-body interaction  $v(\vec{r}_1, \vec{r}_2)$ , and dashed lines the one-body mean-field potential  $v_{m.f.}(\vec{r})$ . Explicit formulas are provided in Appendix A.

It should be noticed that, in order to have a nontrivial  $P_{[1/1]}[G_0]$ , we must have  $\Sigma_1 \neq 0$ , otherwise  $P_{[1/1]}[G_0] = G_0$ . This is the case, for instance, of the self-consistent Hartree-Fock Green's function  $G_{\text{HF}}$ , for which higher order Padé approximants must be considered in order to have a nontrivial correction to  $G_{\text{HF}}$ .

The Green's function of real systems is often calculated on a truncated orbital basis  $\{u_{i\sigma}(\vec{r})\}$  and Fourier transformed to frequency space. If such a basis diagonalizes the matrix  $H_0 = T + V_{\text{ext}} + V_{m.f.}$ , then  $G_0$  can be expressed as a diagonal matrix whose components are

$$g_{ij}(\omega) = \delta_{ij} \begin{cases} \frac{1}{\omega - i\eta + (\epsilon_j - \epsilon_0)} & j \in \mathcal{O} \\ \frac{1}{\omega + i\eta - (\epsilon_j - \epsilon_0)} & j \in \mathcal{U} \end{cases}, \quad (18)$$

where  $\mathcal{O}$  denotes the set of occupied orbitals, while  $\mathcal{U}$  the set of unoccupied ones,  $\epsilon_0$  the ground-state energy, and  $\epsilon_j$  the energy of the  $j$ th orbital; the above diagrammatic expression (17) then reduces to

$$\Sigma_{ij}^{(1)} = \sum_{k \in \mathcal{O}} (v_{ikkj} - v_{ikjk}) - i\delta_{ij} v_{ii}^{m.f.} \quad (19)$$

$$\begin{aligned}
\Sigma_{ij}^{(2)}(\omega) &= \sum_{o,q,r} \mathcal{O}_q \left( \frac{\mathcal{O}_o \mathcal{M}_r}{\epsilon_o + \epsilon_r} + \frac{\mathcal{O}_r \mathcal{M}_o}{\epsilon_r + \epsilon_o} \right) (v_{iojr} - v_{iorj})(v_{qroq} - v_{qrqo}) \\
&+ \sum_{nps} v_{isnp}(v_{npsj} - v_{npsj}) \left( \frac{\mathcal{O}_s \mathcal{M}_n \mathcal{M}_p}{\omega + i\eta - \epsilon_s - \epsilon_n - \epsilon_p} + \frac{\mathcal{O}_n \mathcal{O}_p \mathcal{M}_s}{\omega - i\eta + \epsilon_p + \epsilon_n + \epsilon_s} \right) \\
&+ \sum_{n,p} (-i) \left( \frac{\mathcal{O}_n \mathcal{M}_p}{\epsilon_n + \epsilon_p} + \frac{\mathcal{O}_p \mathcal{M}_n}{\epsilon_p + \epsilon_n} \right) (v_{injp} - v_{inpj}) v_{pn}^{m.f.}
\end{aligned} \tag{20}$$

where  $\mathcal{O}_i$  ( $\mathcal{U}_i$ ) is 1 if  $i \in \mathcal{O}$  ( $i \in \mathcal{U}$ ) or 0 otherwise,  $v_{ijkl}$  is defined by

$$\int d\vec{r} d\vec{r}' u_{i\sigma}^*(\vec{r}) u_{i\lambda}^*(\vec{r}') v(|\vec{r} - \vec{r}'|) u_{m\mu}(\vec{r}') u_{nv}(\vec{r}) = v_{ilmn} \delta_{\lambda\mu} \delta_{\sigma\nu} \tag{21}$$

for which  $v_{jilm} = v_{ijml}$  and

$$\int d\vec{r} u_{i\sigma}^*(\vec{r}) v_{m.f.}(\vec{r}) u_{j\rho}(\vec{r}) = v_{ij}^{m.f.} \delta_{\sigma\rho} \tag{22}$$

defines  $v_{ij}^{m.f.}$ . By switching to the matrix notation

$$\begin{aligned}
\{G_{ij}(\omega)\} &\rightarrow \mathbf{G}, \quad \{g_{ij}(\omega)\} \rightarrow \mathbf{G}_0, \quad \{\Sigma_{ij}^{(1)}(\omega)\} \rightarrow \mathbf{\Sigma}_1, \\
\{\Sigma_{ij}^{(2)}(\omega)\} &\rightarrow \mathbf{\Sigma}_2
\end{aligned} \tag{23}$$

one can readily apply formula (14) to calculate the finite version of (15) in frequency domain.

We notice that the writing (15) suggests that such an approximation can be cast in terms of *two* Dyson equations. Suppose we write

$$\begin{aligned}
G(1, 2) &= G_0(1, 2) + \int d3d4 G_0(1, 3) \Sigma(3, 4) G(4, 2) \\
\Sigma(1, 2) &= \Sigma_1(1, 2) + \int d3d4 \Sigma_1(1, 3) \Xi(3, 4) \Sigma(4, 2).
\end{aligned} \tag{24}$$

The approximant  $P_{[1/1]}[G_0]$  is then obtained by approximating the kernel  $\Xi$  with

$$\Xi(1, 2) \approx \int d3d4 \Sigma_1^{-1}(1, 3) \Sigma_2(3, 4) \Sigma_1^{-1}(4, 2). \tag{25}$$

More generally, the approximant  $[n/n]$  can be expressed as the solution of a set of  $n + 1$  Dyson-like equations. For  $n \rightarrow \infty$  the solution of such a hierarchy of Dyson equations can be regarded as a continued fraction representation of the Green's function.

When solved by iteration, the second equation of (24) with the approximation (25) gives rise to the approximate expansion for the self-energy:

$$\begin{aligned}
\Sigma &\approx \Sigma_1 + \Sigma_2 (\Sigma_1^{-1} \Sigma_2 + \Sigma_1^{-1} \Sigma_2 \Sigma_1^{-1} \Sigma_2 \\
&+ \Sigma_1^{-1} \Sigma_2 \Sigma_1^{-1} \Sigma_2 \Sigma_1^{-1} \Sigma_2 + \dots).
\end{aligned} \tag{26}$$

Although each term is of well defined order in  $\lambda$ , the formal parameter introduced to generate the perturbative expansion as in (8), they do not correspond to specific diagrams. More generally, kernels of the hierarchy of Dyson equations will always be combinations of terms of the perturbative expansion

of the self-energy, but, while the latter can be expressed diagrammatically, the former cannot. As we can see already in (25), this is due to the fact that, although products of diagrams are diagrams themselves, not all products of diagrams and inverse of diagrams are always expressible as diagrams too. The standard diagrammatic picture is therefore unsuitable to give a physical interpretation to such approximations.

Finally, we would like to comment about the computational cost of (15) and compare it with that of higher order approximants. We observe that the calculation of the first nontrivial order  $P_{[1/1]}[G_0]$  for a real system requires: (i) the calculation of a truncated basis set, (ii) the calculation of  $v_{ijkl}$  given in (21), (iii) the calculation of  $\Sigma_{ij}^{(1)}$  and  $\Sigma_{ij}^{(2)}$  via formulas (19) and (20), (iv) the calculation of (14) and then of  $G$  using the Dyson equation, or, equivalently, of (13). Usually the first step, if numerical, is performed by modern codes quite efficiently even for large basis sets; numerical computation and storage of  $v_{ijkl}$ , which involves a double integration on coordinate space for each element of a four-index tensor, can, on the other hand, be quite demanding; once that is available, computation and storage of  $\Sigma_{ij}^{(1)}$  and  $\Sigma_{ij}^{(2)}$  is less expensive, while the last step, which involves a matrix inversion, can also be an onerous task, according to the size of the basis set required for convergence. Now, suppose you want to calculate the next order  $P_{[2/2]}[G_0]$ . Assuming that the basis set is already sufficiently large, the cost of the second and fourth points remains unaltered for the greatest part [the only difference being an undramatic extension of (14) or (13)]. The main difference is calculating higher orders of the expansion of the self-energy, which requires more diagrams than those contained in expressions (19) and (20). Such a number increases exponentially, which means that at a certain point it will overcome the computational cost of (ii) and (iv). However, for sufficiently low orders, this is still accessible (see for instance [4] and references therein), making approximants like  $P_{[2/2]}[G_0]$  probably still at hand.

### III. PERFORMANCE ON HUBBARD RINGS

#### A. The model

The Hubbard model [5], with its many incarnations and variants, is widely used in condensed matter physics for being a sufficiently simple model and yet reflecting many properties of real materials. Its relevance for this work stems from the fact that in some simplified setups it can be exactly solved (at least numerically) while still representing a nontrivial many-body problem. Here we consider  $L$  number of contiguous sites

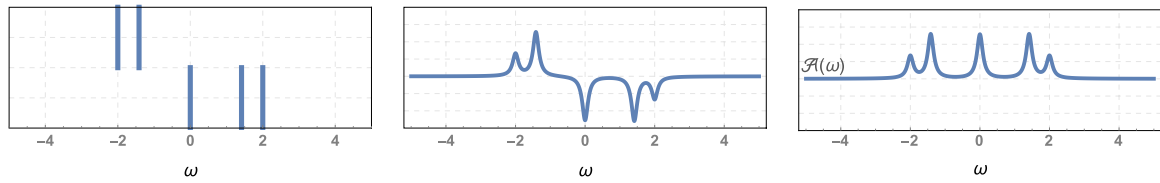


FIG. 1. The spectral function of the Green's function is a collection of infinite peaks, here pictorially depicted in the first panel. When the  $\eta$  parameter is considered finite, one has a sum of Lorentzian functions in the upper ('removal peaks') and the lower half plane ('addition peaks'), as in the second panel. The smoothed spectral function, for which also addition peaks lie on the upper half plane, is depicted in the last panel. The absolute scale of these spectral functions is irrelevant, as it depends on the unphysical  $\eta$  parameter, and from here on values on the y axis will always be omitted.

filled with  $N \leq 2L - 2$  particles subject to the Hamiltonian:

$$H = -t \sum_{(i,j),\sigma} \hat{c}_{i\sigma}^\dagger \hat{c}_{j\sigma} + U \sum_i \hat{c}_{i\uparrow}^\dagger \hat{c}_{i\uparrow} \hat{c}_{i\downarrow}^\dagger \hat{c}_{i\downarrow}, \quad (27)$$

where  $\hat{c}_{i\sigma}^{(\dagger)}$  is an annihilation (creation) operator of a fermion of spin  $\sigma$  on a site  $i$  and  $(i, j)$  denotes the sum over contiguous sites (two per site, in our one-dimensional setting), with periodic boundary conditions (which make it a so-called 'Hubbard ring'). Each site can accommodate up to two particles of opposite spin; particles can hop to neighboring sites with an energy gain of  $-t$ , while double occupancy of a site is disfavored by a repulsive on-site interaction  $U$ . The zero-temperature Green's function of the model can be written as

$$\begin{aligned} G_{i\sigma j\rho}(\omega) &:= \langle GS | \hat{c}_{i\sigma}(\omega + i\eta - (\hat{H} - \langle GS | \hat{H} | GS \rangle))^{-1} \hat{c}_{j\rho}^\dagger | GS \rangle \\ &+ \langle GS | \hat{c}_{j\rho}^\dagger(\omega - i\eta + (\hat{H} - \langle GS | \hat{H} | GS \rangle))^{-1} \hat{c}_{i\sigma} | GS \rangle, \end{aligned} \quad (28)$$

while the noninteracting one  $G_0$  is defined as  $\lim_{U \rightarrow 0} G$ .

For a sufficiently low number of sites  $L$ , the function (28) can be calculated numerically. In particular, we used a code [6,7] that relies on the Lanczos algorithm [8] for  $L = 4, 6, 8, 10$  and  $N = 2, 4, \dots, 2L - 2$ . The choice of having only states with an even number of particles, which in their lowest energy configuration distribute in an unpolarized configuration for which  $G_{i\uparrow j\downarrow}(\omega) = G_{i\downarrow j\uparrow}(\omega) = 0$  and  $G_{i\uparrow j\uparrow}(\omega) = G_{i\downarrow j\downarrow}(\omega) := G_{ij}(\omega)$ , has the purpose of avoiding possible additional features due to spin polarization.

### B. Goodness criterion

To establish the goodness of an approximation to  $G$  we adopt a quantitative criterion based on the error in estimating the corresponding spectral function  $A$ , defined as:

$$A(\omega) := \frac{2}{\pi} \left| \text{Im} \left[ \sum_i G_{ii}(\omega) \right] \right|. \quad (29)$$

Strictly speaking, the Green's function in the spectral representation,  $G_{ij}(\omega)$ , is a distribution represented by a series of so-called 'addition' (+) and 'removal' (-) poles

$$\frac{\alpha}{\omega - \omega_0 \pm i\eta} \quad (30)$$

with some real  $\alpha$  and  $\omega$  and an infinitesimal positive parameter  $\eta$  that serves as a reminder of the position of the pole in the complex plane when integrating over the frequency  $\omega$ . In order to have integrals over smooth functions we: (i) consider a finite value of  $\eta$ , for definiteness  $\eta = 0.1$ , which makes finite the height and width of the peak and (ii) switch all poles to the upper part of the complex plane, by setting  $\alpha/(\omega - \omega_0 - i\eta) \rightarrow \alpha/(\omega - \omega_0 + i\eta)$ , which makes all peaks positive avoiding the derivative discontinuity that we would have had if we had simply taken the absolute value. This procedure, illustrated in Fig. 1, allows us to define the 'smoothed' spectral function

$$\mathcal{A}(\omega) := \frac{2}{\pi} \text{Im} \left[ \sum_i G_{ii}(\omega) \right] \Big|_{-i\eta \rightarrow +i\eta} \quad (31)$$

with  $\eta = 0.1$ . From that, we define the *average absolute deviation*  $\sigma$  as follows:

$$\sigma := \frac{\int d\omega |\mathcal{A}_{\text{exact}}(\omega) - \mathcal{A}_{\text{approx}}(\omega)|}{\int d\omega |\mathcal{A}_{\text{exact}}(\omega)|}. \quad (32)$$

This will be used as a parameter to quantify the goodness of an approximation: the higher is  $\sigma$ , the worst will be considered the corresponding approximation. In Fig. 2 we report a particularly neat example, the case with  $L = 6, N = 2, U/t = 4$  that illustrates the connection between the parameter  $\sigma$  and the intuitive notion of 'good approximate spectral function,' also providing a visual scale of reference for some representative values of  $\sigma$ . The criterion is obviously somehow arbitrary, for certain details of the spectral function (position of the quasiparticle peaks, existence of satellites,...) may be of greater importance in certain situations; nonetheless it is general enough to provide an indication of the behavior of the three approaches under study under generic circumstances.

Concerning the calculation of the approximate spectral functions, two remarks are in order. First, G-PT leads to approximate Green's functions that cannot be written in terms of poles [9], while  $\Sigma$ -PT and dP-PT always lead to approximations that can be reduced to the sum of poles, even though we do not always do it in practice, the effects being negligible [10]. Second, in case of degeneracy, the expression (20) can be divergent, but we found that introducing a simple cutoff  $\epsilon$  in formula (20) as  $(\epsilon^+ - \epsilon^-) \rightarrow (\epsilon^+ - \epsilon^- + \epsilon)$  and setting it to zero after the calculation of the Green's function is sufficient to always get a finite result [11].

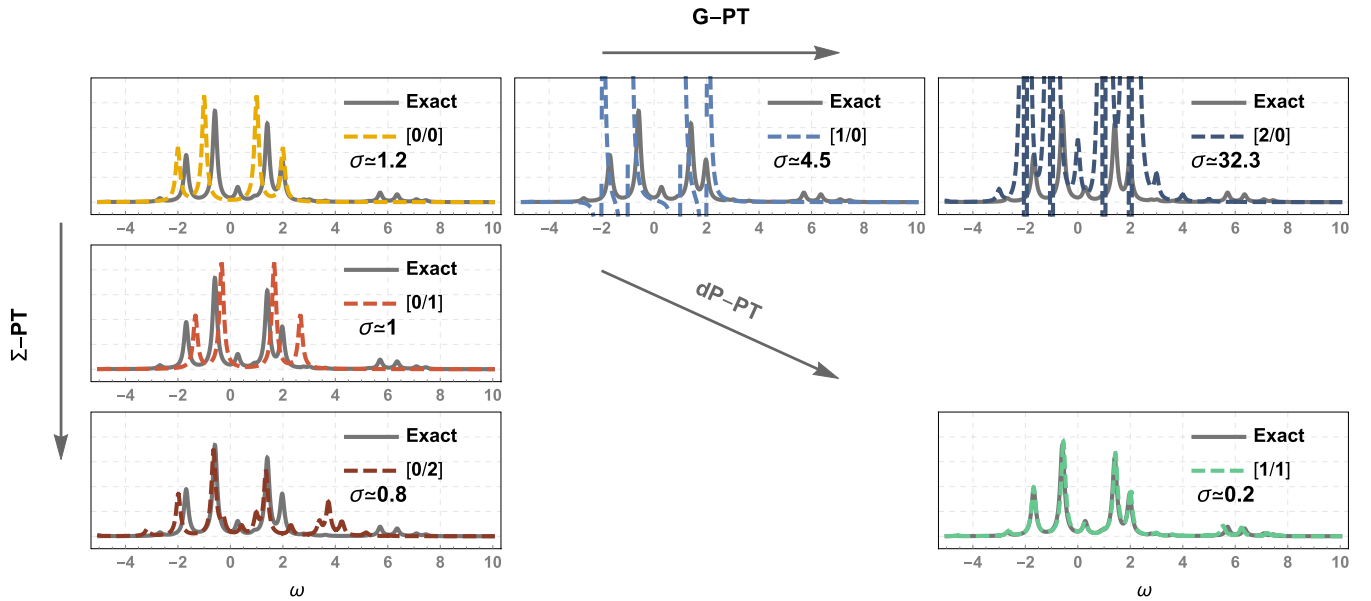


FIG. 2. The function  $\mathcal{A}(\omega)$  is here plotted for different approximations in the case  $L = 6, N = 2, U/t = 4$ .

### C. Choice of the basis

The Green's function of the Hubbard model (28) has been here defined in the so-called 'site' basis. Any Bogolioubov transformation of the ladder operators induces a new basis, which results in a rotation of the matrix  $\{G_{ij}(\omega)\}$ . The choice of the basis does not affect the spectral function, which is calculated from the trace of the Green's function. However, Padé approximants built in different basis are inequivalent. This raises the question: Is there a basis in which Padé approximants (not necessarily diagonal ones but also G-PT and  $\Sigma$ -PT) work better? To attempt to reply to this question, we looked at the case of  $L = 2$ , also known as Hubbard 'dimer.'

For two sites the model is simple enough to admit an analytic solution and in Appendix B we show the ground states, labeled by the number of particles  $\langle \hat{N} \rangle$  and, in case of degeneracy, the spin polarization  $\langle \hat{S}_z \rangle$ . Padé approximants can be calculated directly from the expression of  $G$  one obtains simplifying (28) with those ground states rather than using many-body perturbation theory (1). This allows us to easily calculate approximants of very high order. Moreover, approximants in a different basis can be calculated by considering rotations of  $G$ . A simple Bogolioubov transformation, reported in Appendix B, is sufficient to make  $G$  diagonal, independently of the number of particles and interaction strength. The fact that such a transformation does not depend on  $U$  implies that also  $G_0$  is diagonal in this basis.

Such a specific basis is particularly relevant because we found that, in the case of the dimer, while G-PT is not affected by a change of basis, both  $\Sigma$ -PT and dP-PT work better in this basis than any other. In fact, dP-PT converged to the exact result in only one step, namely  $P_{[1/1]}[G_0] = G$ , for  $L = 2, N = 0, 1, 2, 3, 4$ , as shown in Appendix B for the representative case  $N = 2$ . Such a remarkable property of this basis for the case  $L = 2$  suggested us to formulate the following conjecture: Padé approximants work best in the basis in which the noninteracting Green's function is diagonal,

irrespective of the number of sites or particles. From now on, we shall assume that and all calculations for  $L > 2$  will be shown only in the basis in which  $G_0$  is diagonal.

### D. Approximations comparison

Combining formulas ((14), (19), (20), (23)) with  $v_{ij}^{m.f.} = 0$  we have an explicit expression for the functional  $P_{[1/1]}$  that also applies to the Hubbard model. Such an approximation is made with the same amount of information (i.e., same diagrams) contained in the second order expansion of  $\Sigma$  or  $G$ , denoted by  $[0/2]$  and  $[2/0]$  in the Padé notation. To compare the behavior of the different expansions G-PT,  $\Sigma$ -PT, and dP-PT we shall then consider the following sequences:

- (i)  $([0/0], [1/0], [2/0])$  for G-PT,
- (ii)  $([0/0], [0/1], [0/2])$  for  $\Sigma$ -PT,
- (iii) and  $([0/0], [1/1])$  for dP-PT.

We have calculated the deviation  $\sigma$ , as defined in (32), for the spectral functions arising from the corresponding approximations to the Green's function, for all rings ( $L = 4, 6, 8, 10$ ) and fillings ( $N = 2, 4, \dots, 2L - 2$ ), in three different regimes of interaction: a weak,  $U = 0.1$ , an intermediate,  $U = 1$ , and a strong coupling,  $U = 10$ , in units of  $t$ . For a given approximation  $[n/m]$  and interaction strength  $U$ , the values of  $\sigma$  for different sites and particles are here plotted on a single panel, arranged as reported in Fig. 3. This allows us to get an idea of a specific approximation for a given interaction strength for all systems considered at a glance. Panels are then grouped for sequence of approximations, G-PT in Fig. 4,  $\Sigma$ -PT in Fig. 5, and dP-PT in Fig. 6. Numerical values are explicitly reported in Appendix C.

Recalling that the closer to 0 (blue in plots) the better is the approximation, we recognize the following trends:

- (i) all approximations deteriorate with increasing  $U$ ;

L=4	N=2		N=4		N=6	
L=6	N=2	N=4	N=6	N=8	N=10	
L=8	N=2	N=4	N=6	N=8	N=10	N=12
L=10	N=2	N=4	N=6	N=8	N=10	N=12
	N=14	N=16	N=18			

FIG. 3. Legend for the panels in the following figures.  $L$  denotes the number of sites, while  $N$  the number of particles.

(ii) varying the number of sites  $L$  does not seem to change the quality of the approximations; a higher number of sites only seems to increase the ‘definition’ of the plots;

(iii) almost all approximations deteriorate when approaching the half-filling case;

(iv) G-PT leads to meaningful results only in the weakly coupling regime, while  $\Sigma$ -PT and dP-PT lead to sensible approximations also in the intermediate and strong one;

(v)  $\Sigma$ -PT seems to have a slow convergence rate; namely the term  $[0/2]$  does not improve over  $[0/1]$  as much as  $[0/1]$  does over  $[0/0]$ ;

(vi) dP-PT seems to have a higher rate of convergence (even when compared with the sequence  $([0/0], [0/2])$ ), especially in the low filling cases ( $N < L$ );

(vii) the higher the  $U$  the better is dP-PT over  $\Sigma$ -PT.

A more direct comparison of  $\Sigma$ -PT and dP-PT is reported in Fig. 7, top panel. As anticipated,  $\Sigma$ -PT is generally worse than dP-PT, especially for low fillings and high values of  $U$ . The cases in which  $\Sigma$ -PT is better are only a few and the improvement is not as much as that of dP-

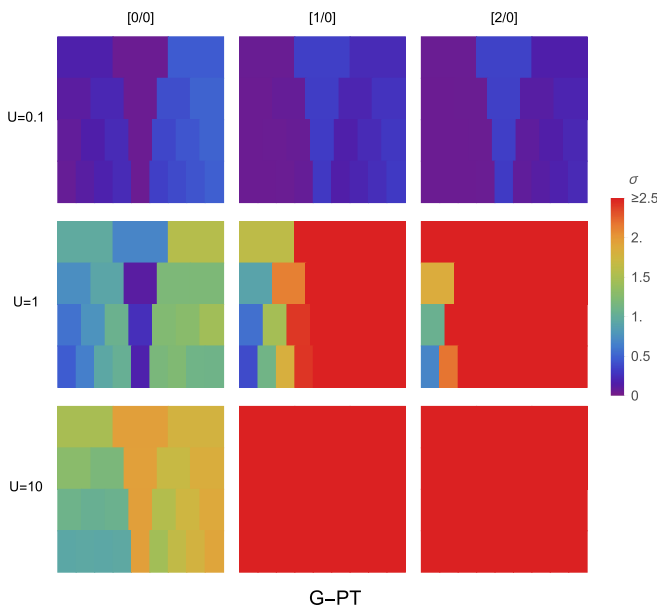


FIG. 4. Average absolute deviation for G-PT approximations.

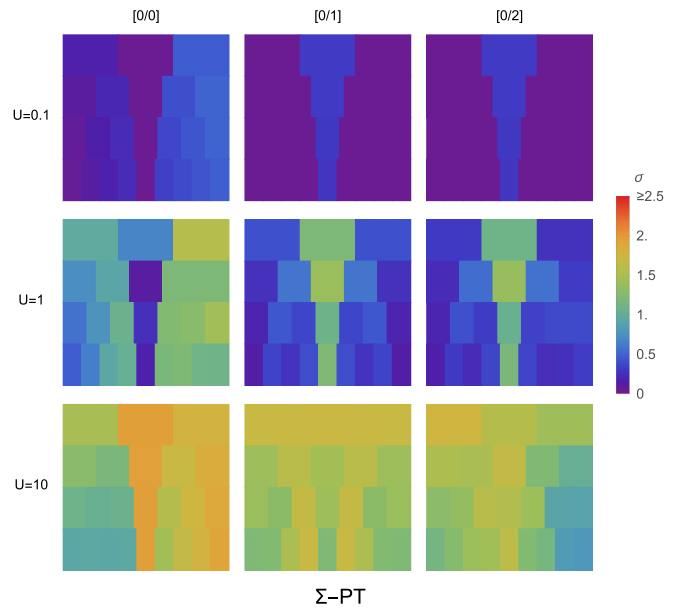


FIG. 5. Average absolute deviation for  $\Sigma$ -PT approximation.

PT in other cases, as exemplified in the bottom panels of Fig. 7.

In absolute terms,  $[1/1]$  leads to a decent approximation in most cases (as seen in Figs. 2 and 7), but, like all other approximations here considered, has serious problems in capturing the half-filling case, as one can see by comparing the first two top curves of Fig. 8. Even though the purpose of our study is to compare dP-PT to other perturbative approaches and not necessarily to provide precise estimates in absolute terms, we would like to focus a bit more on the half-filling case which in general (i.e., not just rings) bares special physical relevance

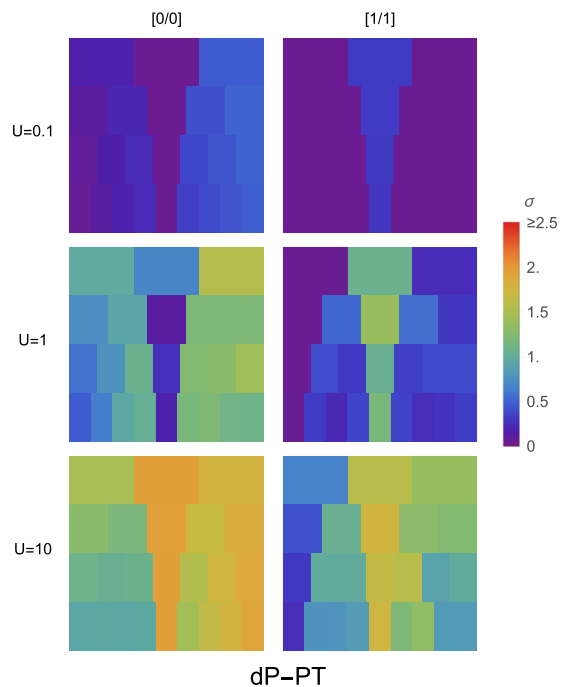


FIG. 6. Average absolute deviation for dP-PT approximations.

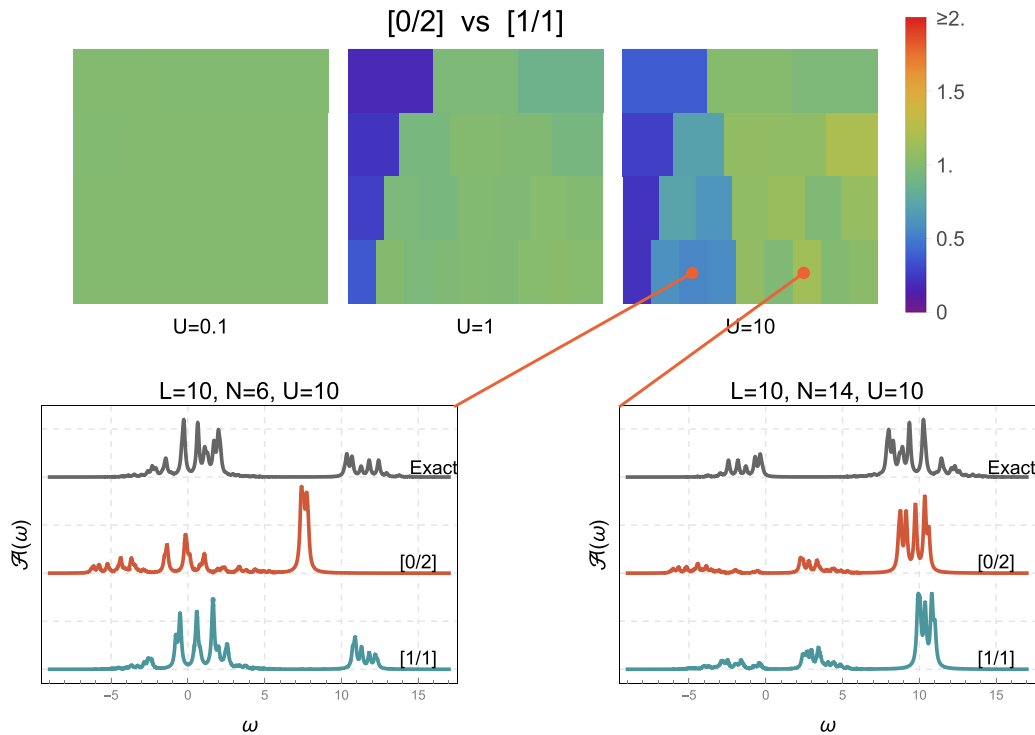


FIG. 7. *Top panel.* The ratio  $\sigma_{[1/1]}/\sigma_{[0/2]}$  is plotted. For most cases this is less than one (green to blue color), indicating that [1/1] provides a better estimate of the exact function than [0/2]. *Bottom panel.* The spectral functions  $\mathcal{A}(\omega)$  in two cases representative of the situations  $\sigma_{[1/1]}/\sigma_{[0/2]} < 1$  and  $\sigma_{[1/1]}/\sigma_{[0/2]} > 1$  are plotted, for a better visual reference of the approximations.

[12]. For instance, for  $L = N = 4$ , the gap, defined as the energy difference between first addition and last removal

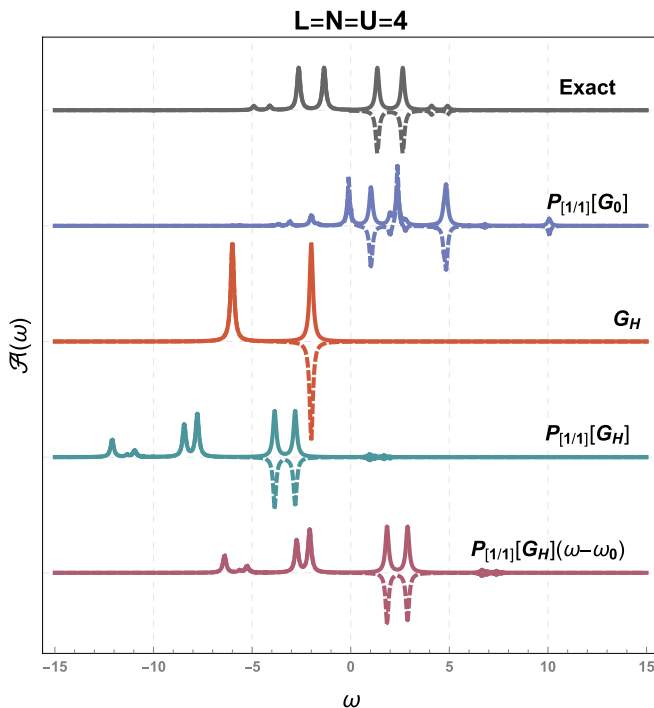


FIG. 8. Various approximated spectral functions are compared to the exact one in the case  $L = N = U/t = 4$ . To distinguish addition from removal peaks, the former are plotted in dashed lines in the lower half of the plane.

peaks, is zero for  $U = 0$  but positive for  $U > 0$ , which can be regarded as a sign of strong correlation. In such a case, shown in Fig. 8 for  $U/t = 4$ , the approximant  $P_{[1/1]}[G_0]$  does not capture the (anti)symmetry of the exact spectrum, nor the fact that addition and removal peaks are well separated by the gap, leading to a spectral function that one may deem as quite far from the exact one. It is legitimate to expect that higher order dP-PT approximants correct these problems and converge towards the exact function, even though we have no elements to actually prove that and, even then, that convergence is practically achievable. On the other hand, for all half-filled systems here considered, we did notice that a sensible improvement comes already from considering a starting point for  $P_{[1/1]}$  different from the pure noninteracting Green's function. By taking  $G_H$ , defined as solution to the equation

$$G_H = G_0 + G_0 \Sigma_H[G_H] G_H \quad (33)$$

with

$$\Sigma_{ij}^{(H)}[g] := - \sum_{kl} \oint \frac{d\omega'}{2\pi} i g_{kl}(\omega') v_{ilkj} \quad (34)$$

and building  $P_{[1/1]}[G_H]$  using formulas ((14), (19), (20), (23)) with  $v_{ij}^{m.f.} = v_{ij}^H = -i\delta_{ij} \Sigma_{ij}^{(H)}[g]$ , one gets to a spectral function that partially restores the (anti)symmetry of the spectral function and correctly opens a gap between addition and removal peaks, as one can see in the penultimate (from top) curve of Fig. 8. Finally, an overall shift with no physical significance can be tuned to give rise to what we would deem as quite a decent approximation to the exact function. By

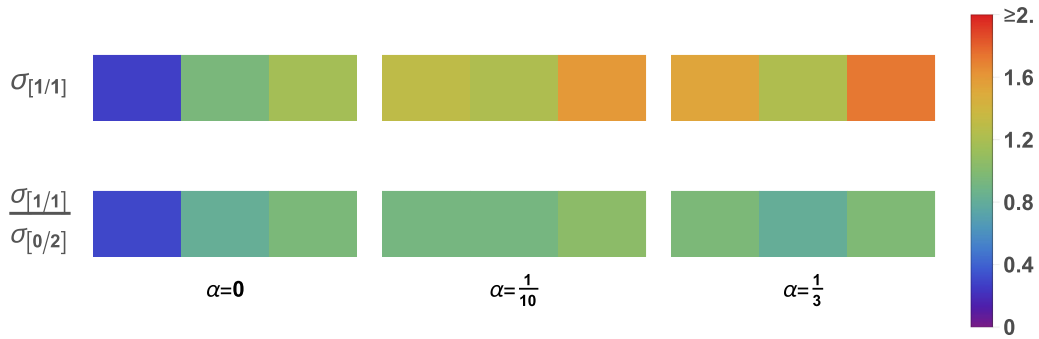


FIG. 9. Effects of a long-range interaction parametrized by  $\alpha$ . Top, performance of [1/1] approximant for increasingly stronger interaction. Bottom, comparison between dP-PT ([1/1]) and  $\Sigma$ -PT ([0/2]).

comparing  $P_{[1/1]}[G_H]$  to  $P_{[0/0]}[G_H]$ , which is simply  $G_H$  (third curve in the plot), it seems then reasonable to expect that of  $P_{[n/n]}[G_H]$  for  $n > 1$  would provide even better approximations to the exact  $G$ .

### E. Beyond the Hubbard model

In view of applications to real systems, the model considered so far represents a good test case for it carries the complexity of the full many-body problem. This, however, is only one of the many ingredients that characterize physical systems. In particular, the on-site interaction of (27) completely neglects any long-range effects of the Coulomb interaction. To move one step closer to real systems, we also considered an off-site interaction by adding to (27) the following term:

$$V = \alpha U \sum_{i=1}^{L-1} c_i^\dagger c_i c_{i+1}^\dagger c_{i+1} \quad (35)$$

which introduces a long-range interaction limited to contiguous sites. The open source SNEG code [13,14] for *Mathematica* [15] was used to create a matrix representation of the new Hamiltonian for  $L = 4$ , which allowed us to calculate the exact Green's functions via (28) for  $N = 2, 4, 6$ ,  $U/t = 4$  and various values of the parameter  $\alpha$ . A higher number of sites were computationally too demanding, but we deem  $L = 4$  as a mild restriction, for we have seen in the previous section that changing the number of sites does not seem to affect the quality of the approximations. In Fig. 9 we present the average absolute deviation of the [1/1] approximant and its comparison with [0/2] for the three representative values of  $\alpha$ : 0, i.e., only on-site interaction, 1/10, and 1/3, a perturbing and a strong off-site interaction, respectively [16]. We can see that in absolute terms the approximation rapidly deteriorates, as soon as the long-range interaction is switched on. In relative terms, however, even though the gap between [1/1] and [0/2] tends to close, [1/1] remains overall a better approximation.

## IV. CONCLUSIONS

Padé approximants have proved to be an effective tool to get estimates of unknown functions in many fields of physics and mathematics [2,17]. Their use in the calculation of electronic properties has been only partially explored, and

in particular in the calculation of Green's functions it has been limited so far as ancillary tool, like for the analytic continuation of the Matsubara Green's functions, or to model systems (see, for instance, Refs. [18–20] and references therein.)

We have here presented a way to build Padé approximants of Green's functions that generalize the standard approximations based on the perturbative expansion of  $G$  or the self-energy  $\Sigma$  and provides a general framework suitable for model as well as for real systems. Moreover, we put forth the conjecture that, among all possible Padé approximants  $[p/q]$  of given order  $p + q$  of the Green's function, diagonal ones,  $p = q$ , offer the best approximation. As a preliminary test, we compared diagonal Padé approximants of order [1/1] against approximations arising from direct perturbative expansion of  $G$  and perturbative expansion of the self-energy of equivalent order for a series of solvable models, namely Hubbard rings with a various number of sites, fillings, and interaction strength, whose exact Green's functions are (numerically) known. Based on a measure of likeness of spectral functions, we found indeed that in general the diagonal Padé approximant offered the most reliable approximation. In the great majority of cases it overcomes the other approximations, for all remaining cases still being quite close to the best (second-order  $\Sigma$ -PT). Particularly good results were obtained for high values of the interaction  $U \gg t$  and low fillings  $N < L$ , irrespectively of the number  $L$  of sites. We also presented a case of physical relevance ( $L = N = U/t = 4$ ) in which the approximant [1/1] built on a mean field, rather than completely noninteracting, Green's function greatly improves the otherwise not so good, in absolute terms, approximation. Finally, to get a better idea on the transferability of these results to real systems, we also performed a study on a simple system in which a long-range interaction was added to the Hubbard on-site one. Performances of dP-PT and  $\Sigma$ -PT on such a system confirm the superiority of the former over the latter and suggest that, in absolute terms, dP-PT may work better on systems with strong on-site interaction, like solids composed of atoms with very localized outer electrons.

Diagonal Padé approximants of the Green's function were not directly built on some physical principle and in fact their physical interpretation as a resummation of certain terms of the perturbative series needs further investigation. On one

hand this might make uncomfortable those who would try to anticipate its behavior on a specific system. On the other hand one can say, in a rather optimistic attitude, that there is great potential in an approximation that is not designed around specific features of a class of systems. The performance of [1/1] on the model studied in this work is a first proof of that.

A more tangible advantage of diagonal Padé approximants [n/n] is that they are systematically improvable by increasing the order  $n$ . In this regard, we also argued that the computational cost increase implied by the rising of the order  $n$  would probably remain moderate for a few orders. This is of capital importance in view of having a reliable, predictive tool.

In fact, the spreading of approximations based on the second-order expansion of the self-energy for a wide range of applications (from nuclear [21] to molecular [22] to periodic systems [23]) suggests that already  $P_{[1/1]}$ , which in our study improves on [0/2] almost in all cases, may already provide a competitive approximation, in all those situations and beyond [24].

In conclusion, we believe that diagonal Padé approximants certainly deserve more attention in the study of the many-body problem, as they may provide an effective new route for designing reliable, systematic approximations within the framework of standard perturbation theory.

## APPENDIX: A

When projected on a basis and Fourier transformed to frequency space, diagrams (17) can be written as:

$$\Sigma_{ij}^{(1)} \equiv \text{diagram 1} + \text{diagram 2} + \dots = \sum_{kl} \oint \frac{d\omega'}{2\pi} i g_{kl}(\omega') (v_{iljk} - v_{ilkj}) - i \delta_{ij} v_{ij}^{m.f.} \quad (\text{A1})$$

and

$$\Sigma_{ij}^{(2)}(\omega) \equiv \Sigma_{ij}^{(2.1)} + \Sigma_{ij}^{(2.2)} + \Sigma_{ij}^{(2.3)} + \Sigma_{ij}^{(2.4)}(\omega) + \Sigma_{ij}^{(2.5)} + \Sigma_{ij}^{(2.6)}(\omega) + \Sigma_{ij}^{(2.7)} + \Sigma_{ij}^{(2.8)} \quad (\text{A2})$$

$$\Sigma_{ij}^{(2.1)} \equiv \text{diagram 2.1} = - \sum_{nopqrs} \oint \frac{d\omega' d\omega''}{4\pi^2} g_{no}(\omega') g_{pq}(\omega'') g_{rs}(\omega') v_{iorj} v_{qsnp} \quad (\text{A3})$$

$$\Sigma_{ij}^{(2.2)} \equiv \text{diagram 2.2} = \sum_{nopqrs} \oint \frac{d\omega' d\omega''}{4\pi^2} g_{no}(\omega') g_{pq}(\omega'') g_{rs}(\omega') v_{iojr} v_{qsnp} \quad (\text{A4})$$

$$\Sigma_{ij}^{(2.3)} \equiv \text{diagram 2.3} = \sum_{nopqrs} \oint \frac{d\omega' d\omega''}{4\pi^2} g_{no}(\omega') g_{pq}(\omega'') g_{rs}(\omega'') v_{iqrj} v_{osnp} \quad (\text{A5})$$

$$\Sigma_{ij}^{(2.4)}(\omega) \equiv \text{diagram 2.4} = - \sum_{nopqrs} \oint \frac{d\omega' d\omega''}{4\pi^2} g_{no}(\omega + \omega' - \omega'') g_{pq}(\omega'') g_{rs}(\omega') v_{isnp} v_{oqjr} \quad (\text{A6})$$

$$\Sigma_{ij}^{(2.5)} \equiv \text{diagram 2.5} = - \sum_{nopqrs} \oint \frac{d\omega' d\omega''}{4\pi^2} g_{no}(\omega') g_{pq}(\omega'') g_{rs}(\omega'') v_{iqjr} v_{osnp} \quad (\text{A7})$$

$$\Sigma_{ij}^{(2.6)}(\omega) \equiv \text{diagram 2.6} = \sum_{nopqrs} \oint \frac{d\omega' d\omega''}{4\pi^2} g_{no}(\omega + \omega' - \omega'') g_{pq}(\omega'') g_{rs}(\omega') v_{isnp} v_{oqjr} \quad (\text{A8})$$

$$\Sigma_{ij}^{(2.7)} \equiv \text{diagram 2.7} = \sum_{nopq} \oint \frac{d\omega'}{2\pi} g_{no}(\omega') g_{pq}(\omega') v_{iojp} v_{qn}^{m.f.} \quad (\text{A9})$$

$$\Sigma_{ij}^{(2.8)} \equiv \text{diagram 2.8} = - \sum_{nopq} \oint \frac{d\omega'}{2\pi} g_{no}(\omega') g_{pq}(\omega') v_{iopj} v_{qn}^{m.f.} \quad (\text{A10})$$

where  $g_{ij}(\omega)$  is the (Fourier-transformed  $ij$  component of) noninteracting Green's function,  $v_{iojp}$  and  $v_{ij}^{m.f.}$  are defined via (21), (22), and the integral is taken over a closed anticlockwise contour large enough to include all poles of the integrand on the upper half of the complex plane. When  $g_{ij}(\omega)$  is written as in (18) those expressions simplify to (19) and (20) by means of the

TABLE I. Groundstates of the Hubbard dimer, categorized by number of particles ( $\langle \hat{N} \rangle$ ), spin polarization ( $\langle \hat{S}_z \rangle$ ), and energy ( $\langle \hat{H} \rangle$ ).

$\langle \hat{N} \rangle$	$\langle \hat{S}_z \rangle$	$\langle \hat{H} \rangle$	$ GS\rangle$
0	0	0	$ 0\rangle$
1	$\frac{1}{2} \cos(2\phi)$	$-t$	$\frac{1}{\sqrt{2}}(\cos(\phi)(\hat{c}_{1\uparrow}^\dagger + \hat{c}_{2\uparrow}^\dagger) + \sin(\phi)(\hat{c}_{1\downarrow}^\dagger + \hat{c}_{2\downarrow}^\dagger)) 0\rangle$
2	0	$\frac{1}{2}(U - \sqrt{16t^2 + U^2})$	$\frac{1}{2}\left(\sqrt{1 - \frac{U}{\sqrt{16t^2 + U^2}}}(\hat{c}_{1\uparrow}^\dagger \hat{c}_{1\downarrow}^\dagger + \hat{c}_{2\uparrow}^\dagger \hat{c}_{2\downarrow}^\dagger) + \sqrt{1 + \frac{U}{\sqrt{16t^2 + U^2}}}(\hat{c}_{1\uparrow}^\dagger \hat{c}_{2\downarrow}^\dagger + \hat{c}_{2\uparrow}^\dagger \hat{c}_{1\downarrow}^\dagger)\right) 0\rangle$
3	$\frac{1}{2} \cos(2\phi)$	$-t + U$	$\frac{1}{2}(\cos(\phi)(\hat{c}_{1\uparrow}^\dagger \hat{c}_{2\uparrow}^\dagger \hat{c}_{2\downarrow}^\dagger - \hat{c}_{1\uparrow}^\dagger \hat{c}_{1\downarrow}^\dagger \hat{c}_{2\uparrow}^\dagger) + \sin(\phi)(\hat{c}_{1\downarrow}^\dagger \hat{c}_{2\uparrow}^\dagger \hat{c}_{2\downarrow}^\dagger - \hat{c}_{1\uparrow}^\dagger \hat{c}_{1\downarrow}^\dagger \hat{c}_{2\downarrow}^\dagger)) 0\rangle$
4	0	$2U$	$\hat{c}_{1\uparrow}^\dagger \hat{c}_{1\downarrow}^\dagger \hat{c}_{2\uparrow}^\dagger \hat{c}_{2\downarrow}^\dagger  0\rangle$

following identities:

$$\oint \frac{d\omega}{2\pi i} g_{jj}(\omega) = \begin{cases} 1 & j \in \mathcal{O} \\ 0 & j \in \mathcal{U} \end{cases} \quad (\text{A11})$$

$$\oint \frac{d\omega}{2\pi i} g_{pp}(\omega) g_{qq}(\omega) = \begin{cases} -\frac{1}{\epsilon_p^- + \epsilon_q^+} & p \in \mathcal{O} \\ & q \in \mathcal{U} \\ -\frac{1}{\epsilon_q^- + \epsilon_p^+} & q \in \mathcal{O} \\ & p \in \mathcal{U} \\ 0 & \text{otherwise} \end{cases} \quad (\text{A12})$$

and

$$\oint \frac{d\omega'}{2\pi i} g_{pp}(\omega' - \omega) g_{qq}(\omega') = \begin{cases} -\frac{1}{\omega - i\eta + \epsilon_q^- + \epsilon_p^+} & p \in \mathcal{U} \\ & q \in \mathcal{O} \\ \frac{1}{\omega + i\eta - \epsilon_p^- - \epsilon_q^+} & q \in \mathcal{U} \\ & p \in \mathcal{O} \\ 0 & \text{otherwise} \end{cases} \quad (\text{A13})$$

which comes from

$$\begin{aligned} & \oint \frac{d\omega'}{2\pi i} \left( \frac{\alpha_1^+}{\omega' - \omega + i\eta + \omega_1^+} + \frac{\alpha_1^-}{\omega' - \omega - i\eta + \omega_1^-} \right) \left( \frac{\alpha_2^+}{\omega' + i\eta + \omega_2^+} + \frac{\alpha_2^-}{\omega' - i\eta + \omega_2^-} \right) \\ &= \frac{\alpha_1^- \alpha_2^+}{\omega + i\eta - \omega_1^- + \omega_2^+} - \frac{\alpha_1^+ \alpha_2^-}{\omega - i\eta + \omega_2^- - \omega_1^+}. \end{aligned} \quad (\text{A14})$$

## APPENDIX: B

In the case  $L = 2$  the Hamiltonian (27) reduces to

$$\hat{H} = -t \sum_{\sigma=\uparrow,\downarrow} (\hat{c}_{1\sigma}^\dagger \hat{c}_{2\sigma} + \hat{c}_{2\sigma}^\dagger \hat{c}_{1\sigma}) + U \sum_{i=1,2} (\hat{c}_{i\downarrow}^\dagger \hat{c}_{i\downarrow} \hat{c}_{i\uparrow}^\dagger \hat{c}_{i\uparrow}). \quad (\text{B1})$$

whose ground states are reported in Table I.

From those one can calculate the Green's function from the definition

$$G_{ij\sigma\rho}(\omega) = \langle \hat{c}_{i\sigma}(\omega + i\eta - (\hat{H} - \langle \hat{H} \rangle))^{-1} \hat{c}_{j\rho}^\dagger \rangle + \langle \hat{c}_{j\rho}^\dagger(\omega - i\eta + (\hat{H} - \langle \hat{H} \rangle))^{-1} \hat{c}_{i\sigma} \rangle. \quad (\text{B2})$$

If this is performed in the basis  $i, j = a, b$ , and  $\sigma, \rho = h, g$ , defined by the transformation

$$\begin{aligned}
\hat{c}_{1\uparrow} &= \frac{(\cos(\frac{\phi}{2}) + \sin(\frac{\phi}{2}))(\cos(\frac{\phi}{2})(\hat{c}_{ah} + \hat{c}_{bh}) - \sin(\frac{\phi}{2})(\hat{c}_{ag} + \hat{c}_{bg}))}{\sqrt{2}\sqrt{\sin(\phi) + 1}} \\
\hat{c}_{1\downarrow} &= \frac{(\cos(\frac{\phi}{2}) + \sin(\frac{\phi}{2}))(\cos(\frac{\phi}{2})(\hat{c}_{ag} + \hat{c}_{bg}) + \sin(\frac{\phi}{2})(\hat{c}_{ah} + \hat{c}_{bh}))}{\sqrt{2}\sqrt{\sin(\phi) + 1}} \\
\hat{c}_{2\uparrow} &= -\frac{(\cos(\frac{\phi}{2}) + \sin(\frac{\phi}{2}))(\sin(\frac{\phi}{2})(\hat{c}_{bg} - \hat{c}_{ag}) + \cos(\frac{\phi}{2})(\hat{c}_{ah} - \hat{c}_{bh}))}{\sqrt{2}\sqrt{\sin(\phi) + 1}} \\
\hat{c}_{2\downarrow} &= -\frac{(\cos(\frac{\phi}{2}) + \sin(\frac{\phi}{2}))(\cos(\frac{\phi}{2})(\hat{c}_{ag} - \hat{c}_{bg}) + \sin(\frac{\phi}{2})(\hat{c}_{ah} - \hat{c}_{bh}))}{\sqrt{2}\sqrt{\sin(\phi) + 1}}
\end{aligned} \tag{B3}$$

then  $G_{ij\sigma\rho} = \delta_{ij}\delta_{\sigma\rho}G_{ij\sigma\rho}$ . In particular, for  $N = 2$  one has

$$G_{aahh} = \frac{\frac{1}{2} - \frac{2t}{\sqrt{16t^2 + U^2}}}{\frac{1}{2}(2t - U + \sqrt{16t^2 + U^2}) - i\eta + \omega} + \frac{\frac{2t}{\sqrt{16t^2 + U^2}} + \frac{1}{2}}{\frac{1}{2}(2t - U - \sqrt{16t^2 + U^2}) + i\eta + \omega} \tag{B4}$$

$$G_{bbhh} = \frac{\frac{1}{2} - \frac{2t}{\sqrt{16t^2 + U^2}}}{\frac{1}{2}(-2t - U - \sqrt{16t^2 + U^2}) + i\eta + \omega} + \frac{\frac{2t}{\sqrt{16t^2 + U^2}} + \frac{1}{2}}{\frac{1}{2}(-2t - U + \sqrt{16t^2 + U^2}) - i\eta + \omega} \tag{B5}$$

$$G_{aagg} = G_{aahh} \quad \text{and} \quad G_{bbgg} = G_{bbhh}. \tag{B6}$$

To construct  $P_{[1/1]}[G_0]$  we can use (14) in the Dyson equation  $\mathbf{G} = \mathbf{G}_0 + \mathbf{G}_0 \mathbf{\Sigma} \mathbf{G}$ , where  $\mathbf{G}_0 = \mathbf{G}|_{U \rightarrow 0}$ . Provided with the exact functional dependence of the Green's function on the interaction parameter  $U$  one can build  $\mathbf{\Sigma}_1$  and  $\mathbf{\Sigma}_2$  either via (A1) and subsequent formulas or, equivalently, directly expanding in Taylor series the function  $\mathbf{G}_0^{-1} - \mathbf{G}^{-1}$ . Upon appropriate rescaling of the infinitesimal parameter  $\eta$ , the two procedures lead to the same results:

$$\mathbf{\Sigma}_1 = \begin{pmatrix} \frac{U}{2} & 0 & 0 & 0 \\ 0 & \frac{U}{2} & 0 & 0 \\ 0 & 0 & \frac{U}{2} & 0 \\ 0 & 0 & 0 & \frac{U}{2} \end{pmatrix} \quad \mathbf{\Sigma}_2 = \begin{pmatrix} \frac{U^2}{4} \frac{1}{\omega - i\eta + 3t} & 0 & 0 & 0 \\ 0 & \frac{U^2}{4} \frac{1}{\omega + i\eta - 3t} & 0 & 0 \\ 0 & 0 & \frac{U^2}{4} \frac{1}{\omega - i\eta + 3t} & 0 \\ 0 & 0 & 0 & \frac{U^2}{4} \frac{1}{\omega + i\eta - 3t} \end{pmatrix} \tag{B7}$$

and

$$\begin{aligned}
& (\mathbf{\Sigma}_1^{-1} - \mathbf{\Sigma}_1^{-1} \mathbf{\Sigma}_2 \mathbf{\Sigma}_1^{-1})^{-1} \\
&= \begin{pmatrix} \frac{U}{2} + \frac{U^2}{4(\frac{1}{2}(6t - U) - i\eta + \omega)} & 0 & 0 & 0 \\ 0 & \frac{U}{2} + \frac{U^2}{4(\frac{1}{2}(-6t - U) + i\eta + \omega)} & 0 & 0 \\ 0 & 0 & \frac{U}{2} + \frac{U^2}{4(\frac{1}{2}(6t - U) - i\eta + \omega)} & 0 \\ 0 & 0 & 0 & \frac{U}{2} + \frac{U^2}{4(\frac{1}{2}(-6t - U) + i\eta + \omega)} \end{pmatrix}
\end{aligned} \tag{B8}$$

which turns out to be the exact self-energy.

### APPENDIX: C

We here report the values, rounded to the second decimal, of the average absolute deviation  $\sigma$  plotted in Figs. 4–7, and 9. See Tables II–VI.

TABLE II. Numerical values plotted in Fig. 4.

	[0/0]	[1/0]	[2/0]
<b>U=0.1</b>	0.17    0.05    0.47	0.06    0.34    0.23	0.05    0.35    0.16
	0.11   0.21   0.05   0.41   0.5	0.05   0.07   0.33   0.19   0.27	0.05   0.05   0.34   0.13   0.19
	0.09   0.16   0.23   0.05   0.37   0.44   0.5	0.05   0.05   0.07   0.32   0.16   0.23   0.3	0.05   0.05   0.05   0.33   0.1   0.15   0.21
	0.07   0.12   0.18   0.23   0.05   0.34   0.39   0.43   0.48	0.05   0.05   0.06   0.07   0.3   0.15   0.2   0.25   0.31	0.05   0.05   0.05   0.06   0.32   0.09   0.13   0.17   0.22
<b>U=1</b>	0.97    0.68    1.57	1.63    3.37    5.5	4.05    13    27
	0.74   0.92   0.12   1.21   1.21	0.9   2.13   3.26   4.7   5.89	1.87   5.74   11   20   31
	0.58   0.77   1.07   0.25   1.24   1.29   1.45	0.56   1.47   2.42   3.14   4.1   4.94   5.85	1.06   3.31   6.6   12   18   25   34
	0.47   0.64   0.94   1.03   0.17   1.18   1.23   1.11   1.1	0.39   1.12   1.83   2.43   2.97   3.84   4.61   5.18   5.82	0.68   2.18   4.33   7.17   11   16   22   28   35
<b>U=10</b>	1.49    1.96    1.79	17    34    50	408    1361    2586
	1.29   1.19   1.95   1.7   1.85	11   22   33   44   55	203   575   1090   2026   3104
	1.09   1.04   1.07   1.96   1.55   1.75   1.89	7.88   16   23   32   40   47   55	121   345   663   1155   1749   2515   3376
	0.93   0.95   0.93   0.95   1.96   1.45   1.65   1.79   1.91	5.91   12   18   24   30   36   42   48   54	80   229   443   728   1079   1588   2161   2806   3517
<b>G-PT</b>			

TABLE III. Numerical values plotted in Fig. 5.

	[0/0]	[0/1]	[0/2]
<b>U=0.1</b>	0.17    0.05    0.47	0.05    0.31    0.05	0.05    0.31    0.05
	0.11   0.21   0.05   0.41   0.5	0.05   0.05   0.32   0.05   0.05	0.05   0.05   0.32   0.05   0.05
	0.09   0.16   0.23   0.05   0.37   0.44   0.5	0.05   0.05   0.05   0.3   0.05   0.05   0.05	0.05   0.05   0.05   0.3   0.05   0.05   0.05
	0.07   0.12   0.18   0.23   0.05   0.34   0.39   0.43   0.48	0.05   0.05   0.05   0.05   0.29   0.05   0.05   0.05   0.05	0.05   0.05   0.05   0.05   0.29   0.05   0.05   0.05   0.05
<b>U=1</b>	0.97    0.68    1.57	0.41    1.21    0.41	0.31    1.1    0.27
	0.74   0.92   0.12   1.21   1.21	0.27   0.59   1.41   0.59   0.27	0.23   0.55   1.38   0.57   0.31
	0.58   0.77   1.07   0.25   1.24   1.29   1.45	0.19   0.45   0.37   1.09   0.37   0.44   0.19	0.2   0.42   0.32   1.05   0.35   0.38   0.38
	0.47   0.64   0.94   1.03   0.17   1.18   1.23   1.11   1.1	0.14   0.35   0.28   0.4   1.22   0.4   0.28   0.35   0.14	0.16   0.31   0.23   0.36   1.19   0.36   0.24   0.26   0.32
<b>U=10</b>	1.49    1.96    1.79	1.69    1.71    1.69	1.75    1.56    1.43
	1.29   1.19   1.95   1.7   1.85	1.42   1.6   1.46   1.6   1.42	1.52   1.5   1.65   1.23   1.03
	1.09   1.04   1.07   1.96   1.55   1.75   1.89	1.4   1.31   1.66   1.42   1.66   1.31   1.4	1.31   1.36   1.59   1.55   1.43   0.91   0.89
	0.93   0.95   0.93   0.95   1.96   1.45   1.65   1.79   1.91	1.22   1.24   1.51   1.7   1.22   1.7   1.51   1.24   1.22	1.15   1.27   1.41   1.45   1.61   1.24   1.16   0.83   0.79
	<b><math>\Sigma</math>-PT</b>		

TABLE IV. Numerical values plotted in Fig. 6.

	<b>[0/0]</b>										<b>[1/1]</b>													
<b>U=0.1</b>	<b>0.17</b>			<b>0.05</b>			<b>0.47</b>				<b>0.05</b>			<b>0.31</b>			<b>0.05</b>							
	<b>0.11</b>		<b>0.21</b>		<b>0.05</b>		<b>0.41</b>		<b>0.5</b>				<b>0.05</b>		<b>0.05</b>		<b>0.32</b>		<b>0.05</b>		<b>0.05</b>			
	<b>0.09</b>	<b>0.16</b>	<b>0.23</b>	<b>0.05</b>	<b>0.37</b>	<b>0.44</b>	<b>0.5</b>				<b>0.05</b>	<b>0.05</b>	<b>0.05</b>	<b>0.3</b>	<b>0.05</b>	<b>0.05</b>	<b>0.05</b>							
	<b>0.07</b>	<b>0.12</b>	<b>0.18</b>	<b>0.23</b>	<b>0.05</b>	<b>0.34</b>	<b>0.39</b>	<b>0.43</b>	<b>0.48</b>				<b>0.05</b>	<b>0.05</b>	<b>0.05</b>	<b>0.05</b>	<b>0.29</b>	<b>0.05</b>	<b>0.05</b>	<b>0.05</b>				
<b>U=1</b>	<b>0.97</b>			<b>0.68</b>			<b>1.57</b>				<b>0.05</b>			<b>1.07</b>			<b>0.23</b>							
	<b>0.74</b>		<b>0.92</b>		<b>0.12</b>		<b>1.21</b>		<b>1.21</b>				<b>0.05</b>		<b>0.52</b>		<b>1.38</b>		<b>0.56</b>		<b>0.29</b>			
	<b>0.58</b>	<b>0.77</b>	<b>1.07</b>	<b>0.25</b>	<b>1.24</b>	<b>1.29</b>	<b>1.45</b>				<b>0.05</b>	<b>0.4</b>	<b>0.3</b>	<b>1.05</b>	<b>0.34</b>	<b>0.39</b>	<b>0.38</b>							
	<b>0.47</b>	<b>0.64</b>	<b>0.94</b>	<b>1.03</b>	<b>0.17</b>	<b>1.18</b>	<b>1.23</b>	<b>1.11</b>	<b>1.1</b>				<b>0.06</b>	<b>0.31</b>	<b>0.22</b>	<b>0.36</b>	<b>1.19</b>	<b>0.36</b>	<b>0.25</b>	<b>0.27</b>	<b>0.33</b>			
<b>U=10</b>	<b>1.49</b>			<b>1.96</b>			<b>1.79</b>				<b>0.65</b>			<b>1.59</b>			<b>1.38</b>							
	<b>1.29</b>		<b>1.19</b>		<b>1.95</b>		<b>1.7</b>		<b>1.85</b>				<b>0.41</b>		<b>1.06</b>		<b>1.78</b>		<b>1.31</b>		<b>1.25</b>			
	<b>1.09</b>	<b>1.04</b>	<b>1.07</b>	<b>1.96</b>	<b>1.55</b>	<b>1.75</b>	<b>1.89</b>				<b>0.3</b>	<b>0.98</b>	<b>0.99</b>	<b>1.65</b>	<b>1.59</b>	<b>0.89</b>	<b>0.98</b>							
	<b>0.93</b>	<b>0.95</b>	<b>0.93</b>	<b>0.95</b>	<b>1.96</b>	<b>1.45</b>	<b>1.65</b>	<b>1.79</b>	<b>1.91</b>				<b>0.25</b>	<b>0.76</b>	<b>0.78</b>	<b>0.84</b>	<b>1.75</b>	<b>1.21</b>	<b>1.33</b>	<b>0.83</b>	<b>0.83</b>			

**dP-PT**

TABLE V. Numerical values plotted in Fig. 7.

										<b>U=0.1</b>					<b>U=1</b>					<b>U=10</b>						
1.			1.			1.			0.18			0.97		0.87		0.37		1.02		0.96						
1.	1.	1.	1.	1.	1.	1.	1.	1.	0.23	0.94	1.	0.99	0.93	0.27	0.7	1.07	1.07	1.21								
1.	1.	1.	1.	1.	1.	1.	1.	1.	0.27	0.95	0.94	1.	0.98	1.02	1.	0.23	0.72	0.62	1.07	1.12	0.98	1.1				
1.	1.	1.	1.	1.	1.	1.	1.	1.	0.36	1.01	0.96	0.98	1.	0.98	1.02	1.03	1.02	0.22	0.6	0.55	0.58	1.08	0.98	1.15	0.99	1.04

**[1/1] vs [0/2]**

TABLE VI. Numerical values plotted in Fig. 9.

$\sigma_{[1/1]}$	0.27	0.95	1.2	1.3	1.2	1.6	1.5	1.2	1.7
$\frac{\sigma_{[1/1]}}{\sigma_{[0/2]}}$	0.3	0.82	0.96	0.92	0.92	1.05	0.96	0.81	0.98
	$\alpha=0$			$\alpha=\frac{1}{10}$			$\alpha=\frac{1}{3}$		

[1] R. Martin, L. Reining, and D. Ceperley, *Interacting Electrons* (Cambridge University Press, Cambridge, 2016).  
 [2] G. Baker and P. Graves-Morris, *Padé Approximants*, Encyclopedia of Mathematics and its Applications (Cambridge University Press, Cambridge, 1996).  
 [3] C. Bender and S. Orszag, *Advanced Mathematical Methods for Scientists and Engineers I: Asymptotic Methods and Perturbation Theory* (Springer, New York, 2013).  
 [4] S. Hirata, A. E. Doran, P. J. Knowles, and J. Ortiz, *J. Chem. Phys.* **147**, 044108 (2017).  
 [5] J. Hubbard, *Proc. Math. Phys. Eng. Sci.* **276**, 238 (1963).  
 [6] G. Alvarez, *Comput. Phys. Commun.* **180**, 1572 (2009).  
 [7] G. Alvarez, “Dmrg++ website” (2009).  
 [8] C. Lanczos, *J. Res. Natl. Bur. Stand. B* **45**, 255 (1950).  
 [9] The underlying mechanism can be illustrated by:

$$\frac{1}{\omega - \omega_0 - i\eta - U} = \frac{1}{\omega - \omega_0 - i\eta} + \frac{U}{(\omega - \omega_0 - i\eta)^2} + \frac{U^2}{(\omega - \omega_0 - i\eta)^3} + \dots,$$

which, despite not being a sum of poles, still converges to the correct result for sufficiently small values of  $U$ .

[10] In the pole representation, the correct solution to the Dyson Eq. (2) can be achieved by considering the function  $\tilde{G} := (G_0^{-1} - \Sigma)^{-1}$  and reducing it to a sum of poles by exploiting the fact that  $\eta$  is not a finite number but rather an infinitesimal. For instance, given  $G_0 = 1/(\omega - i\eta)$  and  $\Sigma = 1/(\omega + i\eta)$ , one has that  $\tilde{G} = 1/(\omega - i\eta - 1/(\omega + i\eta))$  which upon reduction to poles becomes  $G = \frac{1/2}{\omega - 1 + i\eta} + \frac{1/2}{\omega + 1 + i\eta}$ . From the computation side, going from  $\tilde{G}$  to  $G$  involves finding the roots of the denominator of  $\tilde{G}$  which can be numerically challenging. A pragmatic way to proceed is to consider  $\tilde{G}$  as an approximation to  $G$  and carry out all calculations with  $\tilde{G}$  rather than  $G$  with a sufficiently small value for  $\eta$ . This is indeed what we have done in our study, where (32) has been evaluated with  $\tilde{G}$ , rather than  $G$ , with  $\eta = 0.1$ .  
 [11] Unravelling the intricacies of perturbation theory on degenerate states lies beyond the purposes of this work, the interested reader being referred to [25].  
 [12] R. T. Scalettar, in *Quantum Materials: Experiments and Theory*, edited by E. Pavarini, E. Koch, J. van den Brink, and G. Sawatzky, Modeling and Simulation (Forschungszentrum Jülich, Jülich, 2016), Chap. 4, pp. 117–147.  
 [13] R. Žitko, *Comput. Phys. Commun.* **182**, 2259 (2011).  
 [14] R. Žitko, “Sneg website” (2014).

- [15] Wolfram Research, Inc., Mathematica, Version 11.3, Champaign, IL (2018), <http://support.wolfram.com/kb/472>.
- [16] To mimic Coulomb's law,  $\alpha$  must be greater than 0 but less than 1. At around  $\alpha = 1/2$  we noticed what seemed to be a crossing of the two lowest eigenvalues of the Hamiltonian, signaling a possible phase transition. To avoid any possible spurious effects, we focused on the range  $0 < \alpha < 1/2$ , for which the choice  $\alpha = 1/10$  seemed quite representative.
- [17] G. A. Baker Jr. and J. L. Gammel, *The Padé Approximant in Theoretical Physics*, Mathematics in Science and Engineering, Vol. 71 (Elsevier Science, New York, 1971).
- [18] D. Z. Goodson, *Wiley Interdiscip. Rev. Comput. Mol. Sci.* **2**, 743 (2012).
- [19] J. Schött, I. L. M. Loch, E. Lundin, O. Grånäs, O. Eriksson, and I. Di Marco, *Phys. Rev. B* **93**, 075104 (2016).
- [20] Y. Pavlyukh, *Sci. Rep.* **7**, 504 (2017).
- [21] V. Somà, T. Duguet, and C. Barbieri, *Phys. Rev. C* **84**, 064317 (2011).
- [22] J. J. Phillips and D. Zgid, *J. Chem. Phys.* **140**, 241101 (2014).
- [23] A. A. Rusakov and D. Zgid, *J. Chem. Phys.* **144**, 054106 (2016).
- [24] It must be noticed that current approaches based on the second-order expansion of the self-energy are generally formulated within a self-consistent formalism, according to which diagrams of the expansion of the self-energy are not written in terms of  $G_0$  but of the fully interacting  $G$  itself. While this alters the diagrammatic content of the generic term  $\Sigma_n$ , formula (16) remains valid and the right-hand side can be read as a functional of  $G$  if  $\Sigma_1$  and  $\Sigma_2$  are too.
- [25] C. Brouder, G. Panati, and G. Stoltz, *Phys. Rev. Lett.* **103**, 230401 (2009).